JOURNAL OF Materials CHEMISTRY

Synthesis and electrochromic properties of mesoporous tungsten oxide†

Wei Cheng,[a] Emmanuel Baudrin,[a] Bruce Dunn[a] and Jeffrey I. Zink[b]

[a]*University of California, Los Angeles, Department of Materials Science and Engineering, Los Angeles, CA 90095, USA*
[b]*University of California, Los Angeles, Department of Chemistry and Biochemistry, Los Angeles, CA 90095, USA*

Received 10th May 2000, Accepted 20th June 2000
First published as an Advance Article on the web 10th October 2000

The electrochromic properties of mesoporous tungsten oxide are described and compared to standard sol–gel films of WO_3. The block copolymer template used in the synthesis was removed by solvent extraction and calcination methods, leading to mesoporous tungsten oxides which range from amorphous to crystalline depending on the removal treatment. The pores are not ordered but do exhibit a fairly regular diameter with an average size of 4 to 5 nm. The mesoporous tungsten oxides exhibit a well behaved electrochromic response and their electrochemical and optical reversibilities are better than those of the analogous sol–gel film. In addition, the mesoporous films exhibit higher rates for coloration and bleaching. The high surface area of these materials is responsible for this behavior and also leads to multiple peaks in the voltammetric scans.

Introduction

Electrochromism offers a relatively simple means of producing variable light transmission by electrochemical oxidation and/or reduction. Over the last several years, electrochromism has received considerable interest for automotive applications (self-dimming rear view mirrors) and "smart" windows as well as for optical displays.[1] Electrochromism has been widely studied in conducting polymer systems (*e.g.*, polythiophene, polypyrrole) and in inorganic oxides (*e.g.*, WO_3, IrO_2, NiO). Among the latter group of materials, WO_3 has received the most attention.[2] WO_3 films have been prepared by a variety of methods including vacuum evaporation,[3] anodic oxidation,[4] spray pyrolysis,[5] sol–gel synthesis,[6,7] sputtering[8] and laser ablation.[9] As a result there is a reasonable understanding of how the preparation method and microstructure influence electrochromic behavior.

The present paper reports the electrochromic properties of mesoporous tungsten oxide films. The ability to form mesoporous oxides based on the use of various structure-directing agents has been widely investigated over the past several years.[10–12] While much of this research has emphasized SiO_2, it is now well established that surfactant templating methods can be extended to a number of other metal oxides including WO_3.[13] There has been only limited study of the functional properties of the non-silicate mesoporous oxides and, thus, there is little understanding of how the presence of pores in the size range of 2 to 20 nm influences the electrical, optical or magnetic properties of the mesoporous material. In the case of mesoporous tungsten oxide, it is interesting to consider how the penetration of electrolyte through the pore network will affect the nature of the electrochromic response. In this paper we compare the properties of tungsten oxide films prepared by sol–gel methods with mesoporous films that use the same chemistry to form the oxide but also incorporate a block copolymer to generate the mesoporous microstructure. The results indicate that the mesoporous material exhibits better kinetics for coloration and bleaching in comparison to standard sol–gel derived tungsten oxide.

†Basis of a presentation given at Materials Discussion No. 3, 26–29 September, 2000, University of Cambridge, UK.

Experimental

Two types of tungsten oxide films were prepared in this study. In one case, sol–gel derived tungsten oxide films were deposited from a coating solution *via* the dip-coating procedure. The solutions were made by reacting 0.98 g WCl_6 (Aldrich) with 10 g anhydrous ethanol as follows:[14]

$$WCl_6 + C_2H_5OH \quad (1)$$

The solution became blue as a small fraction of W^{VI} reduced to W^V.[15] After stirring for several hours, the sol was filtered to make the final coating solution. ITO coated glass (15 $\Omega\ \square^{-1}$) was used as the film substrate. The dip coating speed was 12.5 mm s^{-1}. The as-deposited film was left in air for one hour to allow the solvent to evaporate and was then fully dried in air at 40 °C. Hydrolysis and condensation of the film occurred from exposure to ambient moisture during the drying treatments.[6,13] To obtain powder samples, the coating solution was dried in an open Petri dish in air at 40 °C for several days.

The second type of film prepared in this study is mesoporous tungsten oxide. (In this paper, the two types of materials are referred to as sol–gel tungsten oxide and mesoporous tungsten oxide to distinguish between the two different types of microstructure.) The coating solution in this case consisted of 0.98 g WCl_6 (Aldrich), 10 g anhydrous ethanol and 0.25 g tri-block copolymer (BASF Pluronic P_{123}) $HO(CH_2CH_2O)_{20}(CH_2CH(CH_3)O)_{70}(CH_2CH_2O)_{20}H$ (designated as $EO_{20}PO_{70}EO_{20}$). The dip-coating and drying conditions were the same as indicated for the sol–gel tungsten oxide. Solvent extraction and calcination methods were used to remove the copolymer. Extraction was accomplished by immersing the films twice into anhydrous ethanol for 10 minutes. Calcination involved heating in air to 300 °C or 400 °C for 2 h at a heating rate of 1 °C min^{-1}.

The sol–gel and mesoporous tungsten oxide materials were characterized by a variety of methods. For the most part, films were characterized. However, in those instances where films were not convenient to use because of the limited amount of material, the corresponding powders were analyzed. The film thickness was measured using an Alpha-step Profilometer. The film was gently scratched to produce the necessary step. X-Ray diffraction (XRD) of the films was carried out on a Crystalogic

 DOI: 10.1039/b003192p

Diffractometer using Cu-K_α radiation ($\lambda = 1.5418$ Å). Transmission electron microscopy (TEM) was performed on a JEOL 2000 electron microscope operating at 200 KeV. The TEM samples were prepared by scratching the film off the substrate, dispersing the particles in ethanol, and depositing them onto a holey carbon film on a Cu grid. Powders (sol–gel and mesoporous) were used for thermogravimetric analysis (TGA 2950; TA Instruments) and nitrogen adsorption–desorption isotherm measurements (Micromeritics ASAP 2000). Chemical analysis of the powders was performed commercially (Galbraith Laboratories).

The electrochemical properties were determined using a three electrode configuration in which the working electrode consisted of the dip coated tungsten oxide film deposited on ITO coated glass. The reference and counter electrodes were a saturated calomel electrode (SCE) and a platinum grid, respectively. The electrolyte was a 0.1 M aqueous solution of sulfuric acid. The voltammetry and chronoamperometry experiments were performed using a PAR 273 potentiostat (EG&G instruments). UV-Visible absorption measurements were performed with a Shimadzu UV-260 spectrophotometer. The transmittance was normalized to 100% at the beginning of the experiment.

Results

Structural and microstructural characterization

The thickness of the tungsten oxide films was in the range of 0.4 to 0.5 μm for all the samples characterized in this work. The compositions of the sol–gel and mesoporous tungsten oxides can be generally written as: $WO_{3-x}\cdot nH_2O$ and $WO_{3-x}\cdot nH_2O\cdot mP_{123}$ respectively. More detailed information concerning the composition was obtained by TGA and chemical analysis as described in the following paragraphs.

The thermogravimetric analysis curve for sol–gel tungsten oxide (Fig. 1a) suggests a three step process: the desorption of adsorbed water between room temperature and 200 °C, the subsequent loss of tightly bonded water molecules between 250 °C and 470 °C, and a gain of oxygen at higher temperature due to the oxidization and crystallization of WO_3. The composition of the as-made sol–gel tungsten oxide can be estimated as $WO_{2.95}\cdot 1.3H_2O$ which is close with the $WO_3\cdot 1.3H_2O$ formula reported by Krings *et al.*[16] who used $WOCl_4$ as the precursor.

The TGA curve of the mesoporous tungsten oxide indicates that the co-polymer is pyrolyzed over the temperature range 140 °C to 350 °C (Fig. 1b). The compositions of the mesoporous tungsten oxides can be estimated as: $WO_{2.94}\cdot 2.8H_2O\cdot 0.011P_{123}$, $WO_{2.94}\cdot 1.3H_2O\cdot 0.001P_{123}$, $WO_{2.94}\cdot 0.8H_2O\cdot 0.0005P_{123}$ and $WO_{2.97}\cdot 0.17H_2O$ for the as-made, solvent extracted, 300 °C calcined and 400 °C calcined samples, respectively. These results show that the co-polymer can be removed to nearly the same extent by solvent extraction as by calcination at 300 °C.

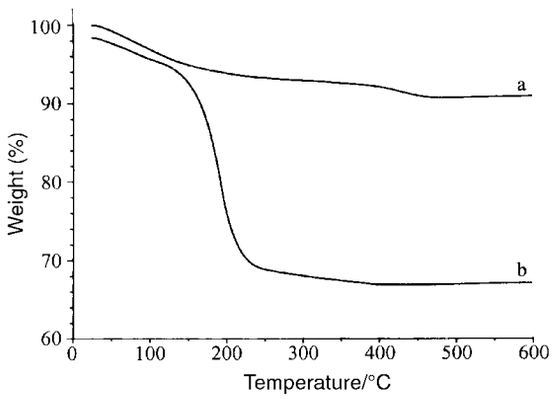

Fig. 1 TGA curves for the (a) sol–gel tungsten oxide and (b) mesoporous tungsten oxide. The samples were heated in air at a rate of 5 °C min^{-1}.

XRD patterns for the sol–gel tungsten oxide and mesoporous tungsten oxide films are compared in Fig. 2. There are some similarities: the as-deposited materials are amorphous while the films heat-treated at 400 °C for two hours crystallize to WO_3. At 300 °C, there is a subtle difference in behavior as the sol–gel film exhibits the onset of crystallization while the mesoporous film is still amorphous.

The morphology of the mesoporous tungsten oxide was characterized by TEM and gas sorption methods. TEM images for extracted and calcined films (Fig. 3a,b) indicate that the pores are not ordered although they do exhibit a fairly regular pore diameter. Pore sizes show a wider distribution (40–80 Å) for the extracted film than for the calcined one (40–60 Å). The TEM images are consistent with the 50% porosity level obtained by gas sorption (Table 1).

Nitrogen adsorption–desorption isotherms (Fig. 3c) exhibit a type IV curve which is characteristic of mesoporous tungsten oxide.[13] The pore size for this material (calcined at 300 °C) showed a fairly narrow distribution, centered at 45 Å (Fig. 3c inset). The surface area (BET), average pore diameter (BJH desorption) and porosity level are listed in Table 1 for the extracted, 300 °C treated and 400 °C treated mesoporous tungsten oxide. The results for the 300 °C treated sample are similar to those reported by Yang *et al.*[13] It would seem that as the calcination temperature increases to 400 °C, the mesopore structure collapses due to the crystallization of the inorganic wall, leading to a decrease in surface area, and an increase in average pore size. In comparison, the sol–gel tungsten oxide material has a smaller surface area ($\sim 20\ m^2\ g^{-1}$ for the dried powder).

Voltammetry and optical measurements

The mesoporous tungsten oxide films exhibit a well behaved electrochemical response (Fig. 4b,c). The voltammograms (from −0.8 V to 0.8 V *vs.* SCE) are similar to those reported in prior studies of proton insertion in tungsten oxide.[16] There is a well-defined anodic peak for the samples calcined at 300 °C and 400 °C and good electrochemical reversibility is observed

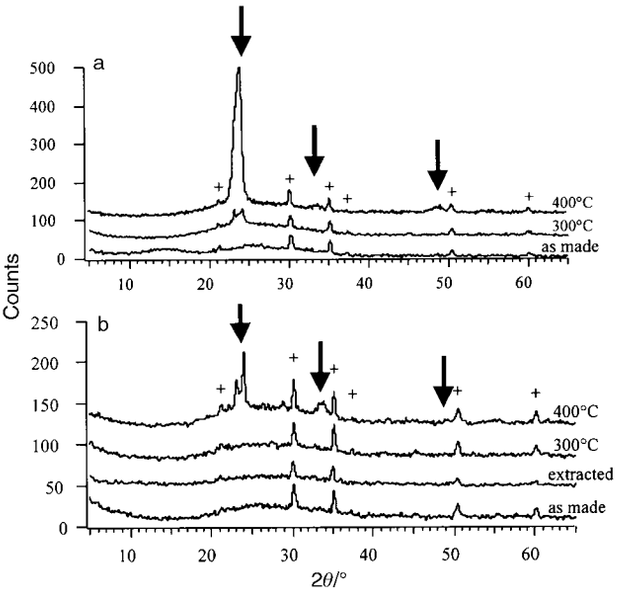

Fig. 2 XRD patterns for (a) sol–gel and (b) mesoporous tungsten oxide thin films heated to different temperatures. The crosses (+) indicate the Bragg peaks from the ITO coating of the substrate and the arrows show the main tungsten oxide peaks.

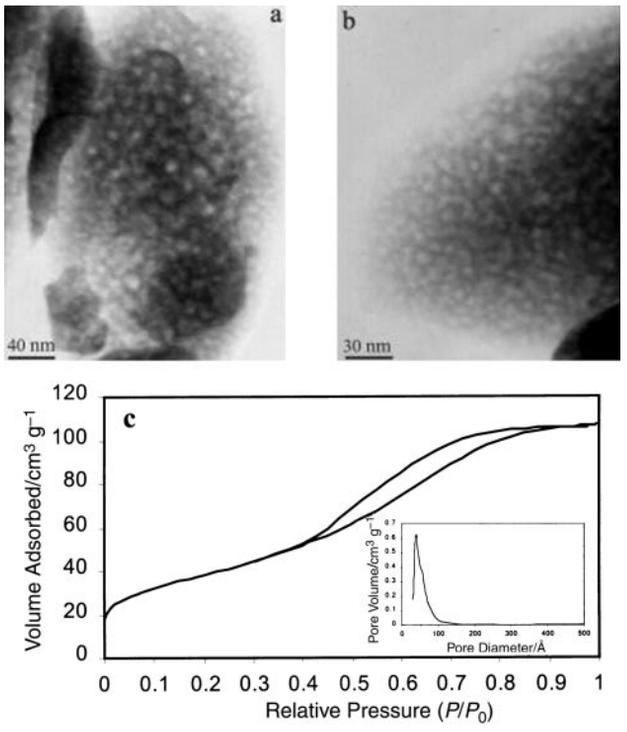

Fig. 3 TEM images of mesoporous tungsten oxide film after (a) ethanol extraction and (b) calcination at 300 °C. (c) Nitrogen adsorption–desorption isotherms and BJH pore size distribution plot (inset) for mesoporous tungsten oxide powder calcined at 300 °C.

after the first cycle. After the fifth cycle, the loss is less than 1% (and most of this loss results from film dissolution, *vide infra*). For comparison, proton insertion in the sol–gel tungsten oxide films leads to significantly more capacity loss, in the range of 50% for the first cycle. The voltammograms (Fig. 4a) do not exhibit well defined anodic peaks and instead are rather featureless over the voltage range. The electrochemical characteristics for the sol–gel and mesoporous films heated to different temperatures are listed in Table 2.

One of the most interesting results obtained with mesoporous tungsten oxide is the development of multiple anodic peaks. Whereas during the first cycle there is only a spike at −0.8 V on reduction and a peak at −0.37 V on oxidation, new features become apparent in the sample calcined at 300 °C after three cycles. There is a new feature in reduction between +0.2 V and −0.2 V and new peaks between +0.1 V and −0.1 V in oxidation. In addition, the original anodic peak is displaced to −0.45 V. The evolution of these changes is shown in Fig. 5a. Electrochemical measurements made on the mesoporous samples prepared by solvent extraction and by calcining at 400 °C provide insight into the origin of this behavior. As shown in Table 1, these two samples exhibit the largest and smallest surface areas, respectively. The mesoporous tungsten oxide prepared by solvent extraction exhibits

Table 1 Surface area, pore size and porosity of the mesoporous tungsten oxide samples

Sample	Surface area[a]/ $m^2\ g^{-1}$	Average pore diameter[b]/Å	Porosity[c]
Solvent extracted	155	50	0.55
300 °C treated	135	45	0.46
400 °C treated	45	106	0.49

[a]BET (Brunauer–Emmett–Teller) method. [b]BJH (Barrett–Joyner–Halenda) desorption. [c]Estimated from pore volume determined by N_2 isotherm curve at $P/P_0 = 0.99$ (single point), and from density measured by a He gas pycnometer (AccuPyc1330, Micromeritics).[13]

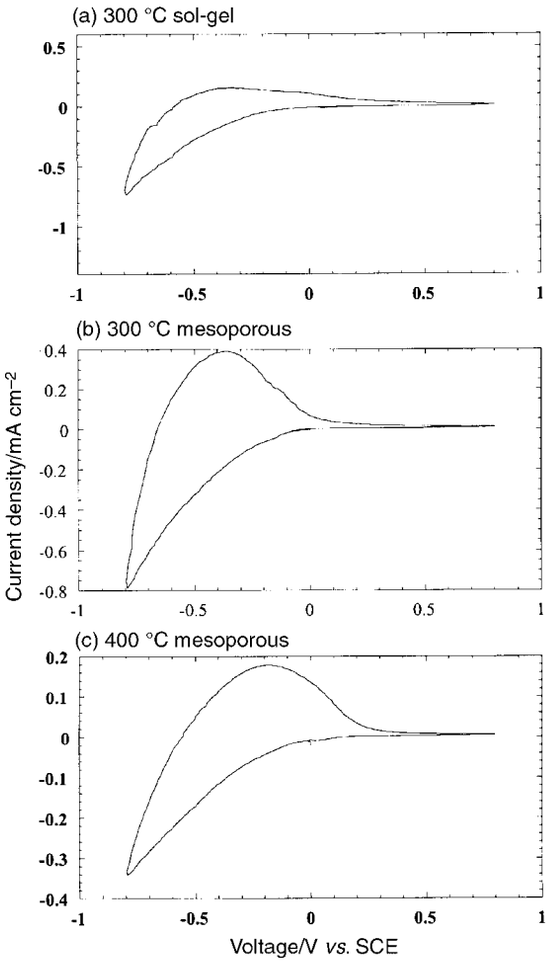

Fig. 4 Voltammetric response for sol–gel tungsten oxide (300 °C calcination) and mesoporous tungsten oxide (300 °C and 400 °C calcination) thin films. The sweep rate was 10 mV s^{-1} and the electrolyte was 0.1 M H_2SO_4.

three anodic peaks during its first cycle at −0.44 V, −0.07 V and +0.18 V (Fig. 5b). That is, no cycling was required to induce this behavior. The 400 °C calcined material (not shown) required electrochemical cycling in order to achieve the evolution of multiple peaks, however, the resolution of the peaks is far less obvious than the results shown in Fig. 5.

The development of multiple peaks during repetitive insertion–deinsertion has been reported previously.[17] Kim and Pyun attributed the three anodic peaks to three types of hydrogen injection sites: reversibly active, shallow trap site (reversible) and deep trap site (irreversible). It would seem that the surface area of the film is an important factor in generating this response. Increasing the surface area will necessarily increase the number of surface active sites; this is one reason that high surface area materials are widely used for catalytic application.[18]

The optical properties of mesoporous tungsten oxide are well behaved in much the same manner as the electrochemical properties. The optical change for the calcined 300 °C sample during the voltammetric sweep is completely reversible (Fig. 6a). There is absorption in the red during reduction as the transmittance at 650 nm decreases to 45%. This change in coloration is completely reversible as the transmittance returns to 100% (normalized value) on oxidation. The ethanol extracted samples show the same behavior. In contrast, the sol–gel tungsten oxide films exhibit much worse reversibility (Fig. 6b). For the sol–gel film heated at 300 °C, re-oxidation leads to 90% transmittance, while the coloration is irreversible (*i.e.*, the films are permanently blue colored) for the as-

Table 2 Voltammetry characteristics for sol–gel and mesoporous tungsten oxide films

Sample[a]	Anodic peak voltage/ V (*vs.* SCE)	Amount of charge intercalated Q_R/C cm^{-2}	Amount of charge deintercalated Q_O/C cm^{-2}	$\Delta Q/Q_R$ (%)[b]
40 °C polymer not removed	−0.37	22.35	12.64	43.5
MP 40 °C ethanol extracted	−0.44	26.45	19.36	26.8
	−0.07			
	+0.18			
MP 300 °C	−0.37	25.98	18.74	27.8
MP 400 °C	−0.19	14.27	9.92	30.5
S–G 40 °C	−0.48	35.26	21.85	38.0
S–G 300 °C	−0.35	24.97	10.65	57.3
S–G 400 °C	−0.10	27.97	14.08	49.7

[a]MP = mesoporous; S–G = sol–gel. [b]First cycle.

deposited sol–gel tungsten oxide and the mesoporous sample heated at 400 °C.

Coloration efficiency and chronoamperometry measurements

In order to provide more insight concerning the nature of the coloration/bleaching processes, two different types of experiments involving the transient response to a voltage step were investigated. The results in Fig. 7 represent the absorption at 650 nm in response to a voltage step applied to a mesoporous film calcined at 300 °C. The step was between −0.8 V and +0.8 V for 30 s and alternated between oxidation and reduction. During the first reduction, the transmittance decreases from 100% to 29% and the time to obtain 50% absorption is 9.2 s. The following oxidation process leads to a completely transparent film in 6.9 s (the transmittance becomes somewhat greater than 100% because of a small amount of film dissolution). That is, the tungsten oxide is slightly soluble in the H_2SO_4 electrolyte.[19] Subsequent cycles show quite good reversibility of the optical properties. In contrast, coloration for sol–gel tungsten oxide is either partially reversible or completely irreversible.

A parameter often used to characterize an electrochromic material is its coloration efficiency (CE) as defined by:

$$CE = \frac{\Delta(OD)}{Q} = \frac{1}{Q} \cdot \log\left(\frac{T_b}{T_c}\right) \quad (2)$$

where Δ(OD) is the variation in optical density, Q the charge density (C cm^{-2}), T_b and T_c the transmittance in the bleached and colored states, respectively. For the mesoporous sample in Fig. 7, a value of 21.2 cm^2 C^{-1} is obtained for the first cycle.

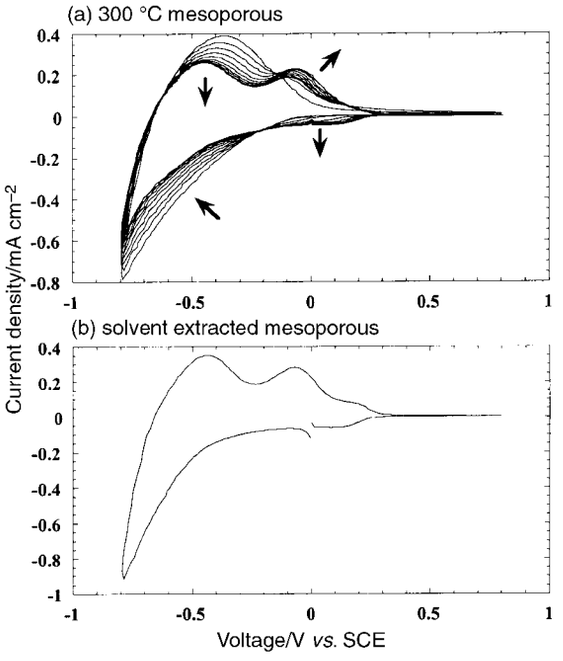

Fig. 5 (a) Evolution of the cyclic voltammogram during cycling for a 300 °C mesoporous tungsten oxide thin film calcined at 300 °C. The arrows show the evolution in the position and intensity of the peaks with cycling. (b) Cyclic voltammogram for solvent extracted mesoporous tungsten oxide (0.1 M H_2SO_4, 10 mV s^{-1}). The sweep rate was 10 mV s^{-1} and the electrolyte was 0.1 M H_2SO_4.

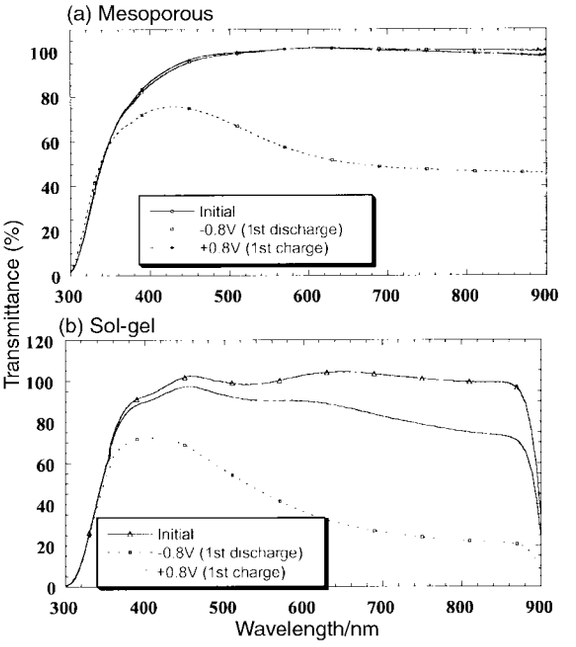

Fig. 6 Optical transmittance spectra for (a) mesoporous and (b) sol–gel tungsten oxide films heated at 300 °C.

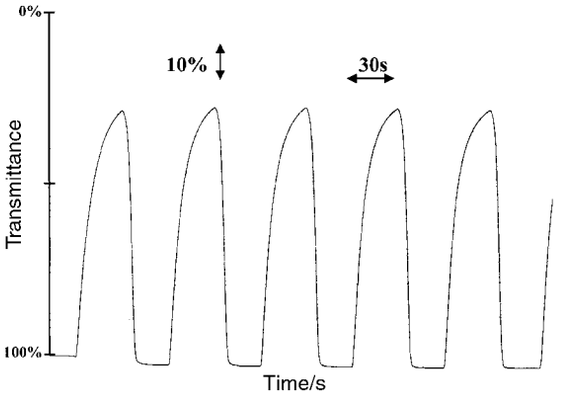

Fig. 7 Variation in the transmittance at 650 nm as a function of time for the mesoporous tungsten oxide films heated at 300 °C and a voltage step between −0.8 V and +0.8 V *vs.* SCE. The voltage changes polarity each 30 s.

Table 3 Coloration time and coloration efficiencies for sol–gel and mesoporous tungsten oxide films

Sample[a]	Coloration time[b]/s	Bleaching time[c]/s	CE (1st cycle)/cm^2 C^{-1}	CE (3rd cycle)/cm^2 C^{-1}	CE (5th cycle)/cm^2 C^{-1}
[a]MP = mesoporous; S–G = sol–gel. [b]Time to obtain 50% change in transmission at 650 nm. [c]Time to obtain original transmission (100%) at 650 nm.					
40 °C polymer not removed	—	Irreversible	16.5	16.3	24.3
MP 40 °C ethanol extracted	9.7	7.5	19.5	21.2	21.6
S–G 300 °C	26.2 (ΔT = 40%)	> 30	17.1	24.4	30.6
MP 300 °C	9.2	6.9	21.2	23	23.5
S–G 400 °C	16.8	> 30	30.7	42.2	43.8
MP 300 °C	26.5 (ΔT = 40%)	> 30	22.7	36.7	35.8

The same experiments have been carried out for the sol–gel and mesoporous tungsten oxide films treated at different temperatures. The results are summarized in Table 3 with the coloration efficiencies calculated for the first, third and fifth cycle. The coloration efficiencies for the first cycle are nearly all in the same range (16–22 cm^2 C^{-1}) and tend to increase somewhat during cycling. These values are close to the typical range (30–50 cm^2 C^{-1}) reported for tungsten oxide.[9] The samples exhibiting the best coloration efficiency are the crystallized films (400 °C).

In the second series of transient experiments, the current response to the voltage step was determined. The responses for sol–gel and mesoporous tungsten oxide films are shown in Fig. 8. The kinetics during coloration (voltage held at −0.8 V for 30 seconds) are approximately the same for both films. However, the bleaching responses (oxidation with the voltage at +0.8 V, from 30 s to 60 s in Fig. 8) are quite different. Whereas the sol–gel tungsten oxide exhibits a gradual decrease in current, the mesoporous film has a two step current decay. In addition, as the films cycle, the decay time for the sol–gel tungsten oxide increases while the mesoporous tungsten oxide response is quite stable. Once again, the mesoporous film exhibits better electrochemical stability than the sol–gel film. Both the ethanol extracted and the 400 °C calcined mesoporous films exhibit the same type of response as that shown in Fig. 8 for the 300 °C mesoporous film.

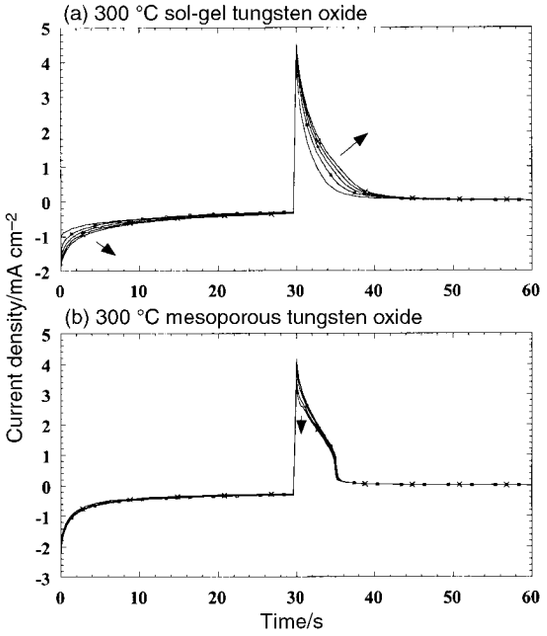

Fig. 8 Chronoamperometry measurements for voltage steps between −0.8 V and +0.8 V (*vs.* SCE) in 0.1 M H_2SO_4 electrolyte; (a) sol–gel tungsten oxide heated at 300 °C and (b) mesoporous tungsten oxide film heated at 300 °C.

Discussion

The studies presented here were directed at establishing the influence of mesoporosity on the electrochemical behavior of tungsten oxide. Accordingly, tungsten oxide materials were prepared by the same synthetic route with the one distinctive difference being that one group of materials was made mesoporous by incorporation of a co-polymer. In general, the mesoporous tungsten oxide films exhibit a well behaved electrochromic response. It is interesting to note that their electrochemical and optical reversibilities are better than those of the analogous sol–gel film and there is evidence that the rate of bleaching is higher. In the following discussion, we review the means by which two microstructural features of the mesoporous film, surface area and porosity, influence the electrochemical behavior.

The evolution of multiple peaks in the voltammetry experiments is a characteristic observed only with the mesoporous samples (Fig. 5). Kim and Pyun,[17] who prepared porous films by magnetron sputtering, proposed that the peaks were associated with proton injection sites. The results shown here correlate with surface area; the film with the greatest surface area (*via* ethanol extraction) exhibited multiple peaks on the first cycle while the calcined samples required some cycling to generate the same response. Since the highest surface area is also expected to possess the greatest number of active sites, the mechanism proposed by Kim and Pyun may be involved with our films as well. A contributing factor here may be surface chemistry. The ethanol extracted films are likely to be rich in hydroxyl groups which may serve as the source of proton injection sites. The calcined materials are expected to have substantially fewer of these groups.

Another characteristic observed for the mesoporous films is the enhanced rates for the coloration and bleaching processes (Table 3). The coloration of tungsten oxide is mainly limited by a barrier at the proton-injecting contact (electrolyte–WO_3 interface).[20] Thus the observed decrease in coloration time (Table 3) can be related to the higher surface area (and increased current) of the mesoporous films as compared to the sol–gel films. Fig. 9a, a log–log plot of the current density (J) as a function of time (t) indicates that the mechanism of coloration is the same for the two types of materials. In Fig. 9a, a slope of −1/2 would correspond to a diffusion limited process. The fact that no such behavior is observed is consistent with previous work where coloration was shown to be controlled by charge transfer.[20]

On the other hand, the bleaching kinetics show an interesting difference for the two types of films. Prior work by Faughnan *et al.*[21] showed that the bleaching current for WO_3 films in H_2SO_4 electrolyte decayed at a rate of $t^{-3/4}$:

$$I(t) = (p^3 \kappa \varepsilon_0 m_p)^{1/4} \cdot V^{1/2} \cdot (4t)^{-3/4} \quad (3)$$

with p the volume charge density of the protons, κ the relative permittivity, ε_0 the permittivity of free space, m_p the proton mobility and V the applied voltage. This response was attributed to a space charge limited current of protons in the film. The space charge region arises from the large difference in

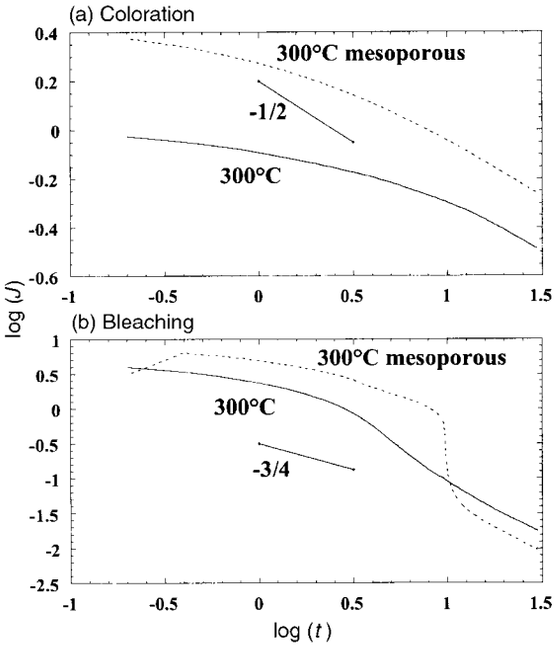

Fig. 9 Log–log plot of current density as a function of time for mesoporous tungsten oxide calcined at 300 °C and sol–gel tungsten oxide heated at 300 °C; (a) coloration (−0.8 V), (b) bleaching (+0.8 V).

mobility between electrons and protons and constitutes the principal contribution to the voltage drop across the film. While both the sol–gel and mesoporous films exhibit the $t^{-3/4}$ transient response, after approximately 10 seconds, the mesoporous film exhibits a sudden current decrease while the sol–gel film shows a gradual change. The sharp decrease in current for the mesoporous material is an indication of the time for complete bleaching to occur.[21] The gradual change observed for the sol–gel film at the end of the bleaching process may be caused by the various factors which influence kinetics at low proton concentrations.[20]

Conclusion

The use of amphiphilic block copolymers as structure-directing agents in systems other than SiO_2 offers the opportunity to create mesoporous transition metal oxide materials with interesting electrochemical and optical properties. This study has shown that mesoporous tungsten oxide exhibits the well known electrochromic properties of this oxide and that the unique microstructure leads to better electrochemical and optical reversibilities with higher rates of coloration/bleaching as compared to standard sol–gel derived tungsten oxide. The improved access of electrolyte to the oxide film *via* the mesoporous texture coupled with the high surface area of the film are factors which contribute to this behavior. Cyclic voltammetry and chronoamperometry measurements suggest that the mesoporous films possess proton trapping sites, a feature which is also expected from the increased surface area. The interesting prospect of increasing the kinetics of electrochromism through the presence of controlled porosity may be of substantial importance for device applications. The nature of the injected ion may also be important. Experiments in progress indicate that lithium insertion and the use of organic electrolytes result in still better reversibility (<10% capacity loss). These results will be the subject of a future report.

Acknowledgements

This material is based upon work supported in part by the U.S. Army Research Office (DAAD 19-99-1-0316) and by the National Science Foundation (DMR-9729186).

References

1 (*a*) C. G. Granqvist, *Handbook of Inorganic Electrochromics Materials*, Elsevier, Amsterdam, 1995; (*b*) P. M. S. Monk, R. J. Mortimer and D. R. Rosseinsky, *Electrochromism: Fundamentals and applications*, VCH, Weinheim, 1995.
2 C. G. Granqvist, *Solar Energy Mater. Solar Cells*, 2000, **60**, 201.
3 O. Bohnke, M. Rezrazi, B. Vuillemin, C. Bohnke, P. A. Gillet and C. Rousselot, *Solar Energy Mater. Solar Cells*, 1992, **25**, 361.
4 A. Dipaola, F. Diquarto and C. Sunseri, *J. Electrochem. Soc.*, 1978, **125**, 1344.
5 R. Hurdich, *Electron. Lett.*, 1975, **11**, 142.
6 P. Judeinstein and J. Livage, *J. Mater. Chem.*, 1991, **1**, 621.
7 O. Lev, Z. Wu, S. Bharathi, V. Glezer, A. Modestov, J. Gun, L. Rabinovich and S. Sampath, *Chem. Mater.*, 1997, **9**, 2354.
8 B. W. Faughnan, R. S. Crandall and P. M. Heyman, *RCA Rev.*, 1975, **36**, 177.
9 A. Rougier, F. Portemer, A. Quédé and M. El Marssi, *Appl. Surf. Sci.*, 1999, **153**, 1.
10 C. T. Kresge, M. E. Leonowicz, W. J. Roth, J. C. Vartuli and J. S. Beck, *Nature*, 1992, **359**, 710.
11 D. Zhao, P. Yang, Q. Huo, B. F. Chmelka and G. D. Stucky, *Curr. Opin. Solid State Mater. Sci.*, 1998, **3**, 111.
12 N. K. Raman, M. T. Anderson and C. J. Brinker, *Chem. Mater.*, 1996, **8**, 1682.
13 (*a*) P. Yang, D. Zhao, D. I. Margolese, B. F. Chmelka and G. D. Stucky, *Chem Mater.*, 1999, **11**, 2813; (*b*) P. Yang, D. Zhao, D. I. Margolese, B. F. Chmelka and G. D. Stucky, *Nature*, 1998, **396**, 152.
14 R. A. Walton, *Prog. Inorg. Chem.*, 1972, **16**, 1.
15 O. J. Klejnot, *Inorg. Chem.*, 1965, **4**, 1668.
16 L. H. M. Krings and W. Talen, *Solar Energy Mater. Solar Cells*, 1998, **54**, 27.
17 D.-J. Kim and S.-I. Pyun, *Solid State Ionics*, 1997, **99**, 185.
18 M. Schneider and A. Baiker, *Catal. Rev. Sci. Eng.*, 1995, **37**, 515.
19 The films are much more soluble in phosphoric acid.
20 (*a*) B. W. Faughnan and R. S. Crandall, in *Display Devices*, ed. J. I. Pankove, Springer, Berlin, Heidelberg, 1980, *Topics in Applied Physics Vol. 40*, p. 181; (*b*) P. M. S. Monk, *Crit. Rev. Solid State Mater. Sci.*, 1999, **24**(3), 193.
21 B. W. Faughnan, R. S. Crandall and M. A. Lampert, *Appl. Phys. Lett.*, 1975, **27**, 275.